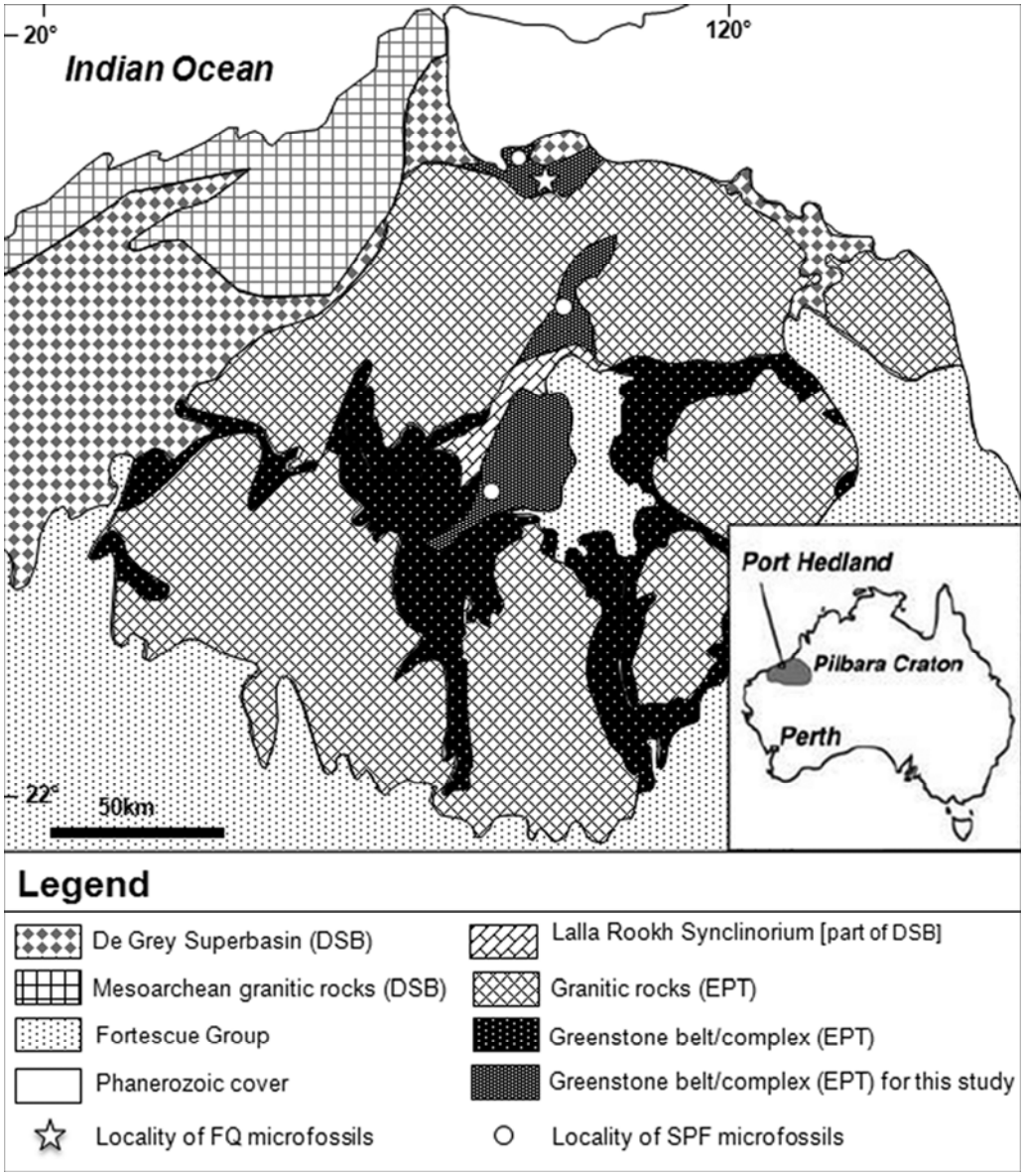

Figure DR1. Location Map for Farrel Quartzite in the Pilbara Craton of northwestern Australia (inset shows location of Pilbara Craton in Australia). Map shows geology of northeastern part of the Pilbara Craton (after Hickman, 2008). DSB and EPT in the legend indicate De Grey Superbasin and East Pilbara Terrane, respectively. A: Panorama greenstone belt; B: Warralong greenstone belt; C: Goldsworthy greenstone belt. Localities for SPF samples with similar microfossils are shown for comparison.

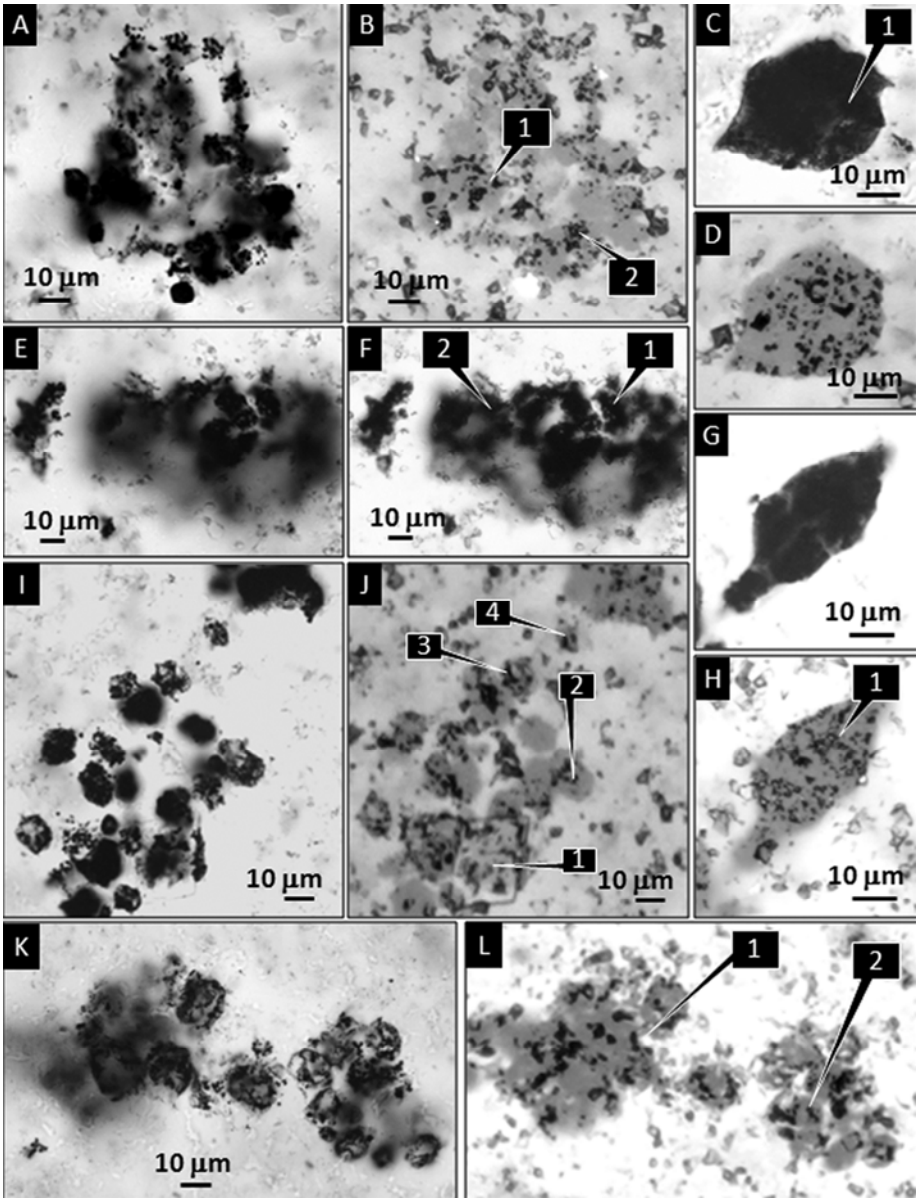

Figure DR2. Optical photomicrographs of additional microfossils in the Farrel Quartzite of Australia – analyzed by SIMS, but not included in Figs. 2-3 in the main text of the paper. A-B, Cluster FQ1_15 of spheroids in transmitted light (A) and reflected light (B). C-D, Spindle FQ1_15 in transmitted light (C) and reflected light (D). E-F, Cluster FQ1_14 in transmitted light ((E) and reflected light (F). G-H, Spindle FQ1_14 in transmitted light (G) and reflected light (H). I-J, Cluster 1 in FQ2_7 in transmitted light (I) and reflected light (J). K-L, Cluster 2 in FQ2_7 in transmitted light (K) and reflected light (L). M-L, Cluster 3 in FQ2_7 in transmitted light (M) and reflected light (N). Note, there is no location 1 in Cluster 3 of FQ2_7. Reflected light images show the locations where SIMS-measured $\delta^{13}C$ values ($\pm 1\sigma$) of analyzed organic matter at the surface. All isotope data are presented in Table S1.

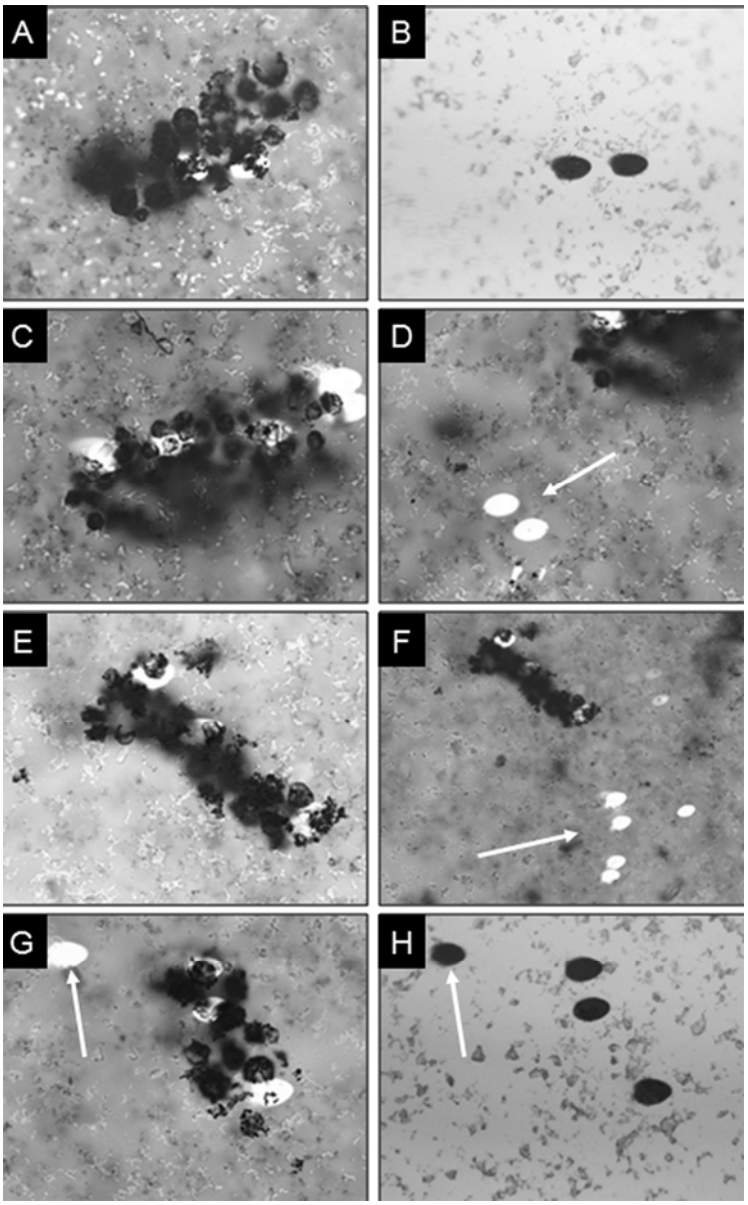

Figure DR3. Optical photomicrographs of spheroidal structures analyzed by SIMS (and illustrated in Fig. 1 of the paper), illustrating SIMS spot sizes, locations of analysis within microfossils, and examples of locations for background analyses. A, C-G are transmitted light micrographs. B and H are the reflected light micrographs of the clusters of spheroids in A and G, respectively. In transmitted light, the SIMS spots generally appear as bright white ovals. In reflected light, the SIMS spots are dark ovals. The reflected light images are helpful for locating the SIMS spots in cases where they may be obscured by the carbonaceous material of the microfossil in transmitted light (see especially the comparison between A and B); that occurs when the SIMS analysis did not penetrate the entire depth of the carbonaceous microfossil (since the transmitted light source shines through the thin section from the bottom to the top). D, F, G and H show some of the SIMS analysis locations that were beyond the clusters of spheroids (arrows) and taken to represent background organic material. D shows background SIMS locations off the lower right end of the cluster in C.

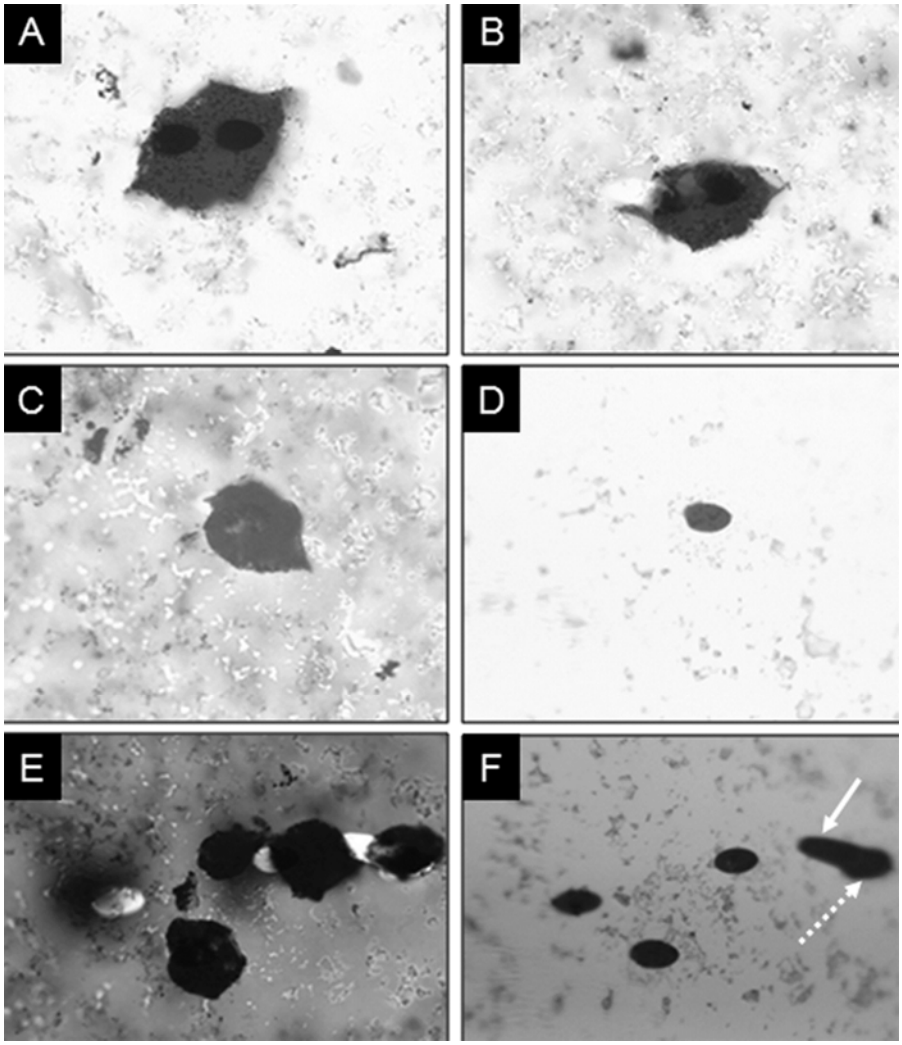

Figure DR4. Optical photomicrographs of spindle-shaped structures analyzed by SIMS (and illustrated in Fig. 2 of the paper), illustrating SIMS spot sizes, locations of analysis within microfossils, and examples of locations for background analyses. A-C, and E are transmitted light micrographs. D and F are the reflected light micrographs of the spindles in C and E, respectively. In transmitted light, the SIMS spots are bright white ovals, except where they are obscured by the carbonaceous material of the spindle (e.g., in A - C). In those cases, the SIMS spots look like dark ovals; that occurs when the SIMS analysis did not penetrate the entire depth of the spindle (since the transmitted light source shines through the thin section from the bottom to the top). In reflected light, the SIMS spots are dark ovals and can be readily seen when they are obscured by the spindle in transmitted light (compare C and D). Solid white arrow in F shows a SIMS spot that missed the spindles, as the center of the analysis spot is between spindles. Dashed arrow in F shows SIMS pot that analyzed the farthest spindle to the right in E.

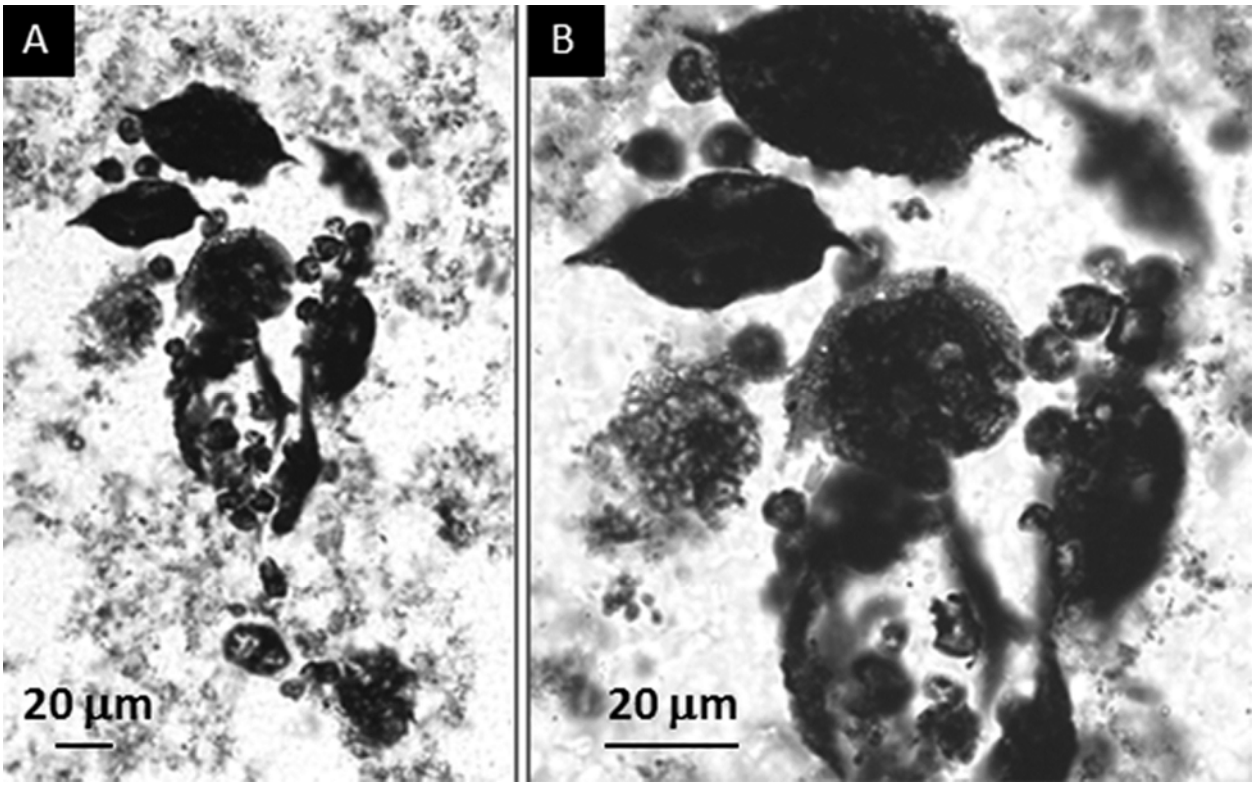

Figure DR5. In exceptional cases, small non-clustered FQ spheres appear to be related and encased and in the large spindle structures. Wide-field (A) and close-up (B) optical image showing mixture of spindles and small spheres. Scale bar is 20 µm.

TABLE DR1. $\delta^{13}C$ VALUES FOR FQ MICROSTRUCTURES AND BACKGROUND SPOTS

Sample ID	Description	$\delta^{13}C$	$\pm\sigma_P$	$\pm\sigma_T$	Cs^+(nA)	C_2 (cps)	Notes
FQ1_4_spchn1	Spindle	-40.5	0.7	1.2	0.03	6.3E+05	Chain of spindles. Location 1, imaged in Figs. 2E-F.
FQ1_4_spchn3	Spindle	-38.4	0.7	1.2	0.03	2.5E+05	Chain of spindles. Location 3, imaged in Figs. 2E-F.
FQ1_4_spchn4	Spindle	-37.2	0.8	1.3	0.03	2.0E+05	Chain of spindles. Location 4, imaged in Figs. 2E-F.
FQ1_4_bkgd@1	Background	-38.3	2.1	2.3	0.03	8.1E+03	Location 1, near spindle chain, FQ1_4.
Bk2_only20cyles	Background	-40.3	5.2	5.3	0.03	1.7E+04	Location 1a, near spindle chain, FQ1_4.
FQ1_4_spchn_bk2	Background	-31.8	1.2	1.6	0.41	9.2E+04	Location 2, near spindle chain, FQ1_4.
FQ1_4_spchn_5	Spindle	-36.3	0.6	1.2	0.05	5.2E+04	Chain of spindles. Location 5, imaged in Figs. 2E-F.
FQ1_15_uni_1	Cluster of spheroids	-33.8	0.7	1.2	0.06	2.6E+05	Location 1 within cluster of FQ1_15, imaged in Supplementary Figs. 2A-B.
FQ1_15_uni_2	Cluster of spheroids	-35.0	0.8	1.3	0.04	2.4E+05	Location 2 within cluster of FQ1_15, imaged in Supplementary Figs. 2A-B.
FQ1_15_sp	Spindle	-35.6	1.2	1.6	0.04	2.1E+05	Single spindle near cluster (FQ1_15), imaged in Supplementary Figs. 2C-D.
FQ1_11_uni_1	Cluster of spheroids	-38.3	0.7	1.2	0.03	5.7E+05	Location 1 in cluster FQ1_11, imaged in Figs. 1A-B.
FQ1_11_uni_2	Cluster of spheroids	-38.6	0.7	1.2	0.03	5.9E+05	Location 2 in cluster FQ1_11, imaged in Figs. 1A-B.
FQ1_14_bk	Background	-28.5	1.7	2.0	0.41	3.3E+04	Location 1, near spindle FQ1-14 of line 17.
FQ1_14_sp	Spindle	-35.6	1.0	1.4	0.03	2.8E+05	Single spindle near cluster (FQ1_14), imaged in Supplementary Figs. 2G-H.
FQ1_14_bk2	Background	-33.5	1.6	1.9	0.41	4.8E+04	Location 2, near cluster FQ1-14 of lines 20-21.
FQ1_14_bk3	Background	-28.5	2.5	2.7	0.40	5.0E+04	Location 3, near cluster FQ1-14 of lines 20-21.
FQ1_14_uni1	Cluster of spheroids	-34.8	0.9	1.3	0.03	3.8E+05	Location 1 within cluster FQ1_14, imaged in Supplementary Figs. 2E-F.
FQ1_14_uni2	Cluster of spheroids	-34.3	1.0	1.4	0.03	5.0E+05	Location 2 within cluster FQ1_14, imaged in Supplementary Figs. 2E-F.
FQ1_10_bk	Background	-29.8	3.9	4.0	0.40	8.0E+03	Location away from microstructures.
FQ1_3_bk	Background	-33.2	11.0	11.0	0.39	9.6E+02	Location away from microstructures.
FQ2_7_bk1	Background	-32.7	1.2	1.5	0.45	1.1E+05	Location 1, in vicinities of clusters of FQ2_7.
FQ2_7_uni_ex	Cluster of spheroids	-34.6	1.0	1.4	0.08	2.5E+05	Location 1 in cluster 1 of FQ2_7, imaged in Supplementary Figs. 2I-J.
FQ2_7_uni_ex2	Cluster of spheroids	-44.2	0.9	1.3	0.03	1.6E+05	Location 2 in cluster 1 of FQ2_7, imaged in Supplementary Figs. 2I-J.
FQ2_7_uni_ex3	Cluster of spheroids	-40.6	0.6	1.1	0.05	4.6E+05	Location 3 in cluster 1 of FQ2_7, imaged in Supplementary Figs. 2I-J.
FQ2_7_uni_ex4	Cluster of spheroids	-41.9	0.9	1.3	0.06	3.3E+05	Location 4 in cluster 1 of FQ2_7, imaged in Supplementary Figs. 2I-J.
FQ2_7_uni_bk2	Background	-34.2	2.5	2.7	0.10	3.6E+04	Location 2, in vicinities of clusters of FQ2_7.
FQ2_7_uni_bk3	Background	-26.0	5.5	5.6	0.45	4.2E+03	Location 3, in vicinities of clusters of FQ2_7.
FQ2_7_uni1_bk	Background	-31.8	1.0	1.4	0.05	2.8E+05	Location near Cluster 2 of FQ2_7.
FQ2_7_uni2	Cluster of spheroids	-34.0	0.7	1.2	0.08	3.0E+05	Location 2 in cluster 2 of FQ2_7, imaged in Supplementary Figs. 2K-L.
FQ2_7_uni3	Cluster of spheroids	-34.1	0.9	1.3	0.07	3.4E+05	Location 3 in cluster 2 of FQ2_7, imaged in Supplementary Figs. 2K-L.
FQ2_5_uni1	Cluster of spheroids	-41.9	1.4	1.7	0.05	8.3E+04	Location 1 in cluster of FQ2_5, imaged in Figs. 1C-D.
FQ2_5_uni2	Cluster of spheroids	-37.3	0.9	1.4	0.06	2.9E+05	Location 2 in cluster of FQ2_5, imaged in Figs. 1C-D.
FQ2_5_uni3	Cluster of spheroids	-36.2	0.8	1.3	0.08	3.4E+05	Location 3 in cluster of FQ2_5, imaged in Figs. 1C-D.
FQ2_5_sp1	Spindle	-36.0	0.6	1.2	0.04	4.0E+05	Location 1 in single spindle of FQ2_5, imaged in Figs. 2A-B.
FQ2_5_sp2	Spindle	-36.4	0.8	1.3	0.13	4.3E+05	Location 2 in single spindle of FQ2_5, imaged in Figs. 2A-B.
FQ2_6_sp1	Spindle	-35.8	0.9	1.3	0.04	3.0E+05	Location 1 in single spindle of FQ2_6, imaged in Figs. 2C-D.
FQ2_6_sp2	Spindle	-36.7	0.9	1.3	0.05	3.1E+05	Location 2 in single spindle of FQ2_6, imaged in Figs. 2C-D.
FQ2_8_uni1	Cluster of spheroids	-34.9	1.0	1.4	0.04	2.1E+05	Location 1 in cluster of FQ2_8, imaged in Figs. 1E-F.
FQ2_8_uni1b	Cluster of spheroids	-36.8	1.0	1.4	0.14	2.6E+05	Location 2 in cluster of FQ2_8, imaged in Figs. 1E-F.
FQ2_8_uni1c	Cluster of spheroids	-35.0	1.1	1.5	0.04	1.9E+05	Location 3 in cluster of FQ2_8, imaged in Figs. 1E-F.
FQ2_8_uni1_bk	Background	-30.3	2.5	2.7	0.24	4.4E+04	Location near the cluster of FQ2_8.
FQ2_9_uni1	Cluster of spheroids	-34.4	0.8	1.3	0.03	4.7E+05	Location 1 in cluster of FQ2_9, imaged in Figs. 1G-H.
FQ2_9_uni2	Cluster of spheroids	-44.2	0.9	1.3	0.04	2.7E+05	Location 2 in cluster of FQ2_9, imaged in Figs. 1G-H.
FQ2_9_uni3	Cluster of spheroids	-35.2	0.9	1.3	0.04	3.1E+05	Location 3 in cluster of FQ2_9, imaged in Figs. 1G-H.
FQ2_9_uni_bk	Background	-34.0	0.6	1.1	0.04	6.2E+05	Location near cluster of FQ2_9.

Notes: σ_P referrs to "primary" uncertainty which here combines in quadrature the internal percision of each analysis with the uncertainty of the instrumental mass factionation (IMF).

$\sigma_P = [(\text{internal percision})^2 + (\text{IMF uncertainty})^2]^{0.5}$, where IMF uncertainty is the standard error on the mean IMF calculated for each day of SIMS work (in this case ±0.3‰).

σ_T refers to a "total" uncertainty, which here combines the σ_P in quadrature with an additional 1‰ standard error approximating the spot-to-spot reproducibility. This term was estimated from the 32 individual analyses of the 215-1 chert standard over the two days. These analyses had an initial Mean Square Weighted Deviation (MSWD) = 1.8. With a 1‰ spot-to-spot uncertainty added in quadrature to the internal percision of each analysis of 215-1, the new MSWD = 1, a value which shows the new total uncertainty matches the variance of the data points. While a spot-to-spot uncertainty of about 1‰ is quite reasonable for SIMS, it may be an overestimation here because repeated analyses of two potential standards (1:1:8 mixes of silica, carbon, and ordinary portland cement) showed no detectable spot-to-spot variation (n = 4; MSWD = 0.1 and n = 5; MSWD = 0.7). For this reason, we have decided to list both estimations of uncertainty in the table, while using the more concervative σ_T in the text of the paper. While these cement mixes being tested did show good isotopic homogenity and yielded good spot-to-spot reproducibility, they were not suitable as a standard because the IMF was found to be quite different than chert (IMF = 21.4±1.1‰ for silica, graphite, and cement; IMF = 20.8±0.9‰ for silica, coal, and cement; compared with IMF = -5.6±0.3‰ for chert PPRG#215-1).

$\text{IMF (‰)} = 1000 * \text{Ln} [(\delta_{exp} + 1000)/(\delta_{obs} + 1000)]$

$\text{MSWD} = \Sigma [(X_{wm} - X_i)^2 / s_i^2] / (n-1)$, where X_{wm} = weighted mean of X, σ_i = standard error in measurement of X_i, and n # of measurements.

$\sigma_T = [(\sigma_P)^2 + (\text{spot-to-spot})^2]^{0.5}$, where spot-to-spot is equal to 1‰ for the work reported here.

A long analysis of the PPRG#215–1 chert at low primary ion beam intensity demonstrated an IMF consistent with our the other analyses of this standard, in line with past SIMS experience using the same conditions. This result, plus the fact that the weighted linear regression of the analyses of PPRG#215–1 as a function of primary ion beam intensity demonstrated no significant slope (≈ -0.5 ‰ per nA), indicates that our overall estimate of IMF is accurate (to a couple of per mil) for all of the FQ results.

Under the conditions used, quasi-simultaneous arrival (QSA) effects are expected to be small because the production of C_2^- is relatively ineffective with ionization around a few percent where carbon is exposed, and to be very similar between the standard chert and the Farrel Quartzite chert because of their similar elemental chemistry. The lack of a QSA isotope effect is supported by analyses of the chert standard, which were consistent over a factor of >5-fold variation in the ratio of secondary ions produced to primary ion current.

Cs^+(nA) is the current of the primary ion beam used.

C_2 (cps) is the detected counts per second for the secondary beam of C^2 ions.